PROFESSOR HAI-LIANG ZHU (Orcid ID : 0000-0001-5254-7487)

Article type : Research Article

Design of Potent B-Raf^{V600E} Inhibitors by MCSS Strategy

Ze-Feng Wang†, Peng-Fei Wang†, Jun-Ting Ma, Ying-Zi Chai, Hui-Min Hu, Wen-Long Gao, Zhong-Chang Wang*, Bao-Zhong Wang*, Hai-Liang Zhu*

State Key Laboratory of Pharmaceutical Biotechnology, Nanjing University, Nanjing 210023, People's Republic of China.

*Corresponding author:

Hai-Liang Zhu, Tel. & fax: +86-25-89682572; e-mail: zhuhl@nju.edu.cn

This article has been accepted for publication and undergone full peer review but has not been through the copyediting, typesetting, pagination and proofreading process, which may lead to differences between this version and the Version of Record. Please cite this article as doi: 10.1111/cbdd.13121

†These two authors contributed equally to this paper.

Abstract

B-Raf kinase is a vital intermedium in the mitogen-activated protein kinase (MAPK) signaling pathway, which transforms extracellular signals into cellular mechanisms. Mutations in this kinase, for instance, the most common V600E mutation, can lead to the ERK signaling pathologically activated and hence cause severe diseases like somatic tumors. So far, the development of B-Raf inhibitors has made remarkable progress. However, the resistance and relapse of approved Raf drugs have been widely reported, and the optimization for old drugs and the discovery for new inhibitors still remain a significant task.

In this study, we designed and evaluated a series of novel B-Raf^{V600E} inhibitors. A fragment library has been established before the docking simulation carried out using the MCSS strategy (multi-copy simulation search). The appropriate fragments were reassembled to provide new candidate compounds, which were further screened by iterative docking simulations and molecular dynamics. Bioassays were carried out to evaluate the pharmacological profile of the compounds identified and synthesized. The result showed that compound **5n** had an impressive enzyme inhibitory and anti-proliferation activity, suggesting a promising potential in the future study.

Key words

MCSS; B-Raf inhibitor; Docking; Molecular dynamics; Bioassays

1 Introduction

Dysfunctions of signaling pathways have long been elucidated to be closely implicated with diverse severe diseases. For instance, when deviation appears in the MAPK (mitogen-activated protein kinase) signaling pathways,[1] it may trigger or promote the process of many human diseases such as amyotrophic lateral sclerosis (ALS), Parkinson's disease (PD), Alzheimer's disease (AD) and various types of cancers.[2-4] While other branches are suggested to mainly mediate neuronal apoptosis in AD, PD, and ALS, the ERK signaling is more connected with tumorigenesis,[5] including cancer cell proliferation, migration, and invasion. In the ERK signaling, Raf is a key component whose mutation will lead to the signaling activated abnormally.[6] The most common mutation observed is B-Raf^{V600E}, as a substitution of glutamate for valine at amino acid 600 (V600E) occurs in the most important subtype of Raf family.[7] This mutation mimics the phosphorylation state, hence the B-Raf^{V600E} protein persistently performs its kinase activity without regulation. The V600E mutation has been detected in most melanomas and some other somatic tumors worldwide, and brings great threat to the health of humans.[8, 9]

Therefore, developing novel B-Raf^{V600E} antagonists keeps a hot topic in the medicinal chemistry industry. With the process of structure elucidation of B-Raf kinase, it’s becoming more feasible to design small molecular inhibitors with favorable features meeting the

requirements to selectively and efficiently suppress the activity of B-Raf^{V600E}.[10, 11] Studies about various kinds of inhibitors have been continually reported. Some of the inhibitors have entered different stages of preclinical or clinical study, and a few already utilized in Raf-related cancer therapy.[12] Much progress has been made, though, the challenge is still uphill: both resistance and relapse have been universally reported when using the known Raf drugs.[13,14] Hence the optimization for old drugs and discovery for new agents remain an important task.

This study presents our recent work on designing and evaluating a new series of B-Raf^{V600E} inhibitor. To begin with, we have established a library of fragments based on the known endogenous ligands extracted from protein-ligand complexes. On the basis of protein structure analysis, the fragments were docked into the active pocket of B-Raf employing MCSS strategy (multiple copy simulation search).[15-18] The fragments with top score and suitable space distribution were recombined to afford the candidate compounds which were redocked to validate, with the binding of the best hit tested by molecular dynamics.[19-21] Afterwards the hit was modified to gain a chemotype diversity and synthesized. Anti-proliferation and kinase inhibition assays *in vivo* were carried out to profile the potency of these derivate entities. The most potent compound **5n**, with IC_{50} values of 0.09 ± 0.002 μM against B-Raf^{V600E} and 0.9 ± 0.17 μM against A375 cell line, was selected to perform western blotting to verify whether the downstream signaling pathway was blocked. Altogether, the results favored our design intention and with this effort, we hope this work will provide more insight in the future research.

2 Results and Discussion

2.1 Chemistry

The synthesis of target compounds followed the general pathway outlined in **Scheme 1**. All of the synthetic compounds are being reported for the first time (**Table S1**) and gave satisfactory analytical and spectroscopic data. ^{1}HNMR, ESI-MS and element analysis spectra were in full accordance with the assigned structures, which were presented in the Supporting Information.

2.1.1 Materials

All chemicals (Analytical grade) used were purchased from Nanjing Chemical Reagent Co. Ltd. (Nanjing, China). All the ^{1}H NMR spectra were recorded on Bruker DPX400 or Bruker DPX600 model spectrometer in DMSO-d_6, and chemical shifts (δ) are reported as parts per million (ppm). ESI-MS spectra were recorded by a Mariner System5304 Mass spectrometer. Elemental analyses were performed on a CHN-O-Rapid instrument and were within 0.4% of the theoretical values. Melting points were determined on a XT4 MP apparatus (Taike Corp., Beijing,China). Thin layer chromatography (TLC) was performed on silica gel plates (Silica Gel60 GF254) and visualized in UV light (254 nm and 365 nm). Column chromatography was performed using silica gel (200 – 300 mesh) and eluting with ethyl acetate and petroleum ether (bp30 – 60 ^{o}C).

2.1.2 Chemistry methods

2.1.2.1 General procedure for the synthesis of compounds (1)

Pyrazole (14.00 g, 205.64 mmol) was dissolved in concentrated H_2SO_4 (50.00 mL). The solution was heated to 60 ^oC, before the dropwise addition of nitric acid (9.20 mL), which caused the temperature rise slightly. The reaction was stirred for 1.5 h at 60 ^oC and poured into 600 g of an ice/water mixture. A white precipitate formed that was filtered and washed with water. This yielded 12.50 g (40%). The filtrate was extracted with ethyl acetate (3 × 100 mL). The combine organic phases were washed with 1% $NaHCO_3$ (aq.100 mL), water (100 mL), and brine (100 mL). Then the ethyl acetate solution was dried over Na_2SO_4 and concentrated *in vacuo*, which yielded another 10.5 g (45%) of the desired product.

2.1.2.2 General procedure for the synthesis of compounds (2a-k)

To a stirred solution of **1** (1.00 g, 8.84 mmol) in DMF (6.00 mL) at 25 ^oC were added K_2CO_3 (1.47 g, 10.60 mmol) and iodomethane (10.60 mmol, 660 μL). After stirring for 16 h at 25 ^oC, the reaction mixture was treated with water (15.00 mL) and EtOAc (20.00 mL) and transferred to a 125 mL separatory funnel. The organic layer was collected and the aqueous layer was extracted with EtOAc (3 × 25 mL). The combined organic layers were washed with brine (20.00 mL), dried over sodium sulfate and filtered. The filtrate was concentrated, and the residue was purified by flash column chromatography to provide the products (for **2a**-**2e**).

A mixture of iodobenzene (6.82 mmol), **1** (0.70 g, 6.20 mmol), 8-hydroxyquinoline (0.09 g, 0.62 mmol), cuprous iodide (0.18 g, 0.62 mmol) and potassium carbonate (1.73 g, 12.40 mmol) in DMSO (10 mL) was heated at 135 ^{o}C for 20 h. After cooling to room temperature, the reaction mixture was diluted with 20 mL of water and extracted with ethyl acetate. The organic layer was washed with aqueous saturated sodium bicarbonate, dried by sodium sulfate, filtered and concentrated *in vacuo*. Purification by flash chromatography gave the desired products (for **2f**-**2i**).

2-bromo-N-(4-methoxyphenyl)acetamide (1.00 mmol, 0.25 g), **1** (1.00 mmol, 0.12 g), sodium ethoxide (0.10 g) was dissolved DMF (50 mL). After stirring for overnight at room temperature, the reaction mixture was treated with water (15 mL) and EtOAc (25 mL). The organic layer was collected and the aqueous layer was extracted with EtOAc (3 × 25 mL). The combined organic layers were washed with brine (20 mL), dried over sodium sulfate and filtered. The filtrate was concentrated, and the residue was purified by flash column chromatography to provide the products (for **2j**-**2k**).

2.1.2.3 General procedure for the synthesis of compounds (3a-k)

Compound **2** (4.00 mmol) was refluxed with ethanol (4.00 mL), 80% hydrazine hydrate (1.00 mL), and 10% palladium charcoal (0.08 g) for 10 min. The reaction was filtered by celite. The filtrate was dried by sodium sulfate, and concentrated *in vacuo* to afford compounds **3a**-**3k**, which were used without further purification.

2.1.2.4 General procedure for the synthesis of compounds (4a-4b)

Methyl 1-methyl-1H-indole-3-carboxylate (or Methyl 1H-indole-3-carboxylate) was added to a solution of potassium hydroxide (1.50 equiv) in water (50 mL). Then the resulting mixture was heated to 65 ^{o}C for 2 h. The resulting solution was cooled, neutralized with dilute hydrochloric acid solution to pH = 5. The precipitated solid was filtered and washed with water to give the product **4a** (or **4b**).

2.1.2.5 General procedure for the synthesis of compounds (5a-5p)

EDC (2.00mmol, 0.38g) was added in one portion to a mixture of **4** (2.00mmol, 1equiv) and HOBt (2.00 mmol, 0.27) in DMF (5.00 mL) at 25 ^{o}C for 30 min. Then a crystal of DMAP (2.00 mmol, 0.25 g), **3** (2.00 mmol), and Et_3N (1 mL) was added and the reaction mixture was stirred overnight. The resulting mixture was poured in water and was extracted with ethyl acetate. Purification by flash chromatography gave the desired products **5a-5p**.

2.2 Data preparation and analysis

Collectively, there were 45 B-Raf co-crystals deposited in the PDB database up to March, 2016 (shown in **Figure S1**). These complexes were downloaded and the correspondingly endogenous ligands were extracted and revised. The receptor protein was primarily prepared with missing amino acid residues and hydrogen atoms added before charged with force field.

By deconstruction, a small library of fragments was established from the original ligand molecules. Afterwards, the fragments were minimized and charged with force field.

2.3 Screening for the best hits

By the MCSS strategy, 2500 ~ 5000 copies for each fragment were randomly distributed and docked into the binding area of the receptor. Low-ranking poses for these fragments were automatically discarded in the output stage and the rest were ordered by the MCSS score. For each fragments, the docking modalities with top scores were collected and recorded. After then, fragments with favorable distribution and orientation were recombined and linked to afford a new skeleton. We used the new skeleton without substituents as a hit compound, and the backbone compound was derivatized to obtain the compounds **5a**-**5p** to discuss structure-activity relationship. Finally, docking simulation was performed to the modified compound, and the CDOCK interaction energy values were depicted in **Figure S2**. The best compound **5n** with highest binding energy (-57.92 kcal/mol) was shown in **Figure 1**. It can be found compound **5n** preferably bound to the active site of the B-Raf^{V600E} (PDB code: **4E26**) by two hydrogen bonds with ILE 527 and CYS 532, and formed three Pi-Pi bonds with TRP531 and PHE 595, along with other weak interactions. Meanwhile, we described the interaction between compound **5n** and B-Raf^{V600E} (PDB code: **4E26**) by the 3D model in **Figure 2A** and an overlay of vemurafinib and compound **5n** with B-Raf^{V600E} (PDB code: **4E26**) has been incorporated in **Figure 2B**. The similarities of conformation distribution between vemurafinib and compound **5n** in B-Raf^{V600E} was suggested in **Figure 2B**, for

example, the distribution of their N, O atoms was similar. The molecular docking suggested that compound **5n** may be a potential B-Raf^{V600E} ligand.

In the **Table S2**, the molecular properties of all the target compounds and vemurafenib have been summarized. In general, B-Raf antagonists have more N, O, S atoms and smaller logP values than other types of antagonists. Therefore, the "Rule of 3" (known as rules for the lead compounds) or "Rule of 5" (known as rules for drug candidates) should be carried out more moderately in the process of designing new B-Raf inhibitors. The recombinant compounds have a smaller molecular weight, less H-donor and acceptor, rotatable bonds and rings than vemurafenib. The comparison is even more obvious when compared with vemurafenib, implying an enormous potential for profile optimization.

With the rapid development of computer technology and molecular computing technology, molecular dynamics simulation has been widely recognized and applied. Molecular dynamics simulation, as an effective post-docking tool, plays a very important role in the verification and optimization of molecular docking. Therefore, in this study we also use the molecular dynamics simulation to test our predicted molecular structure. As an example, **Figure 3** showed that B-Raf-ligand **5n** systems settled into equilibrium state soon after the start of simulation, with fluctuations wobbling in narrow ranges. Also, the RMSD values showed that ligand **5n** in the system was quite stable. Together the virtual simulations suggested these compounds bear promising potential, and the best hits were thereafter synthesized and evaluated for their biological efficiency.

For the molecular dynamics simulation results, equilibrium state simulation of 8.0 ns - 10.0 ns were selected, and the energy composition was extracted every 100 ps. The MM/PBSA free binding energy was analyzed for the 20 samples. MM/PBSA free binding energy is mainly composed of van der Waals force, electrostatic force, polar solvation and non-polar Solvation. For this system, the average energy and free binding energy of the system are shown in **Table 1**. The results showed that van der Waals played a major role in the binding process of ligand and protein (-250.43 $\pm$ 4.33 kJ/mol), and the total free binding energy of protein and ligand summed up to -219.40 $\pm$ 10.41 kJ/mol. The results indicated that the binding of small molecules to receptors was better.

2.4 Compound 5n potently inhibited B-Raf^{V600E} kinase activity and proliferation of cancer cells

The inhibitory effects of test compounds **5a-5p** on kinase B-Raf^{WT}, B-Raf^{V600E} and C-Raf were evaluated using vemurafenib as a positive control drug. In the **Table S3** and **Table S4**, it can be seen that both compound **5n** and vemurafenib showed impressive enzymatic inhibition to B-Raf^{V600E} kinase (with IC_{50} values of 0.10 $\pm$ 0.01 μM and 0.03 $\pm$ 0.007 μM, respectively). Their inhibitory effect toward wild-type B-Raf has decreased, compared to B-Raf^{V600E} kinase (with IC_{50} values of 0.92 $\pm$ 0.02 μM and 0.22 $\pm$ 0.018 μM, respectively). Vemurafenib is a potent pan-Raf inhibitor (IC_{50} value of 0.19 $\pm$ 0.018 μM against C-Raf), and compound **5n** has a weak inhibitory effect on C-Raf with an IC_{50} value of 6 times that of vemurafenib (IC_{50} value of 1.09 $\pm$ 0.081 μM). The other compounds also exhibited good efficacy, even though not as effective as the positive control drug vemurafenib and **5n** (**Table S3** and **Table S4**).

The entities were evaluated for their anti-proliferation activities against four cancer cell lines, HT29 (B-Raf^{V600E}), A375 (B-Raf^{V600E}), WM1361 (B-Raf^{WT}), and HCT116 (B-Raf^{WT}), by the MTT assay, and the calculated IC_{50} values were shown in **Table S3.** To compound **5n**, it showed better suppression compared with vemurafenib when exerting on the A375 cells and HT29 cells for 48 h (with IC_{50} values of 0.93 $\pm$ 0.11 μM and 2.27 $\pm$ 0.21 μM against IC_{50} values of 1.08 $\pm$ 0.26 μM and 1.56 $\pm$ 0.24 μM, respectively). To WM1361 and HCT116 cells cells expressing B-Raf^{WT}, the cell viability of cells treated with compound **5n** and vemurafenib was significantly higher than that of cells carrying B-Raf^{V600E}. The MTT assays suggested that the compound **5n** is a potential B-Raf^{V600E} inhibitor and could efficiently inhibit the proliferation of B-Raf^{V600E}-harbored cell lines.

It can be seen from the **table S3** that when R^1 substituent was constant, the change in R^2 substituent had a crucial effect on the activity of the compounds. Comparing compound **5a** with **5l**, **5c** with **5m**, **5g** with **5n**, **5h** with **5o**, and **5j** with **5p**, we can easily draw the following conclusions: when there was the same R^1 substituent, compounds with different R^2 substituent groups were compared, and it was clear that the activity of the tested compounds with different R^2 substituent decreased obviously in the following order: -H > -CH_3. It is shown that N-methylated are less potent than the corresponding NH free compounds. When R^2 substituent was constant, R^1 substituent biological activities of different inhibitors declined with the following order: *p*-tolyl > phenyl > methoxyphenyl > the remaining other substituents. Though other compounds are less potent, many are close to the control.

2.5 Compound 5n induced cell apoptosis in dose- and time-dependent manner

Reports have revealed that vemurafenib could induce cell apoptosis. To verify whether compound **5n** has the similar apoptosis-inducing effect, a cell apoptotic experiment on compound **5n** was carried out. It is clear from the results that compound **5n** could induce cell apoptosis. Experimental results showed that after treating A375 cells with gradient concentrations (0 μM, 1 μM, 3 μM and 10 μM) of compound **5n** for 24 h, the percentage of apoptotic cells was markedly elevated in a dose-dependent manner (with percentage of 3.547%, 8.27%, 56.80% and 58.50%). The results indicated that after treating A375 cells with gradient times (0 h, 12 h, 24 h and 36 h) of compound **5n** for 3 μM, the percentage of apoptotic cells was markedly elevated in a dose-dependent manner (with percentage of 0.681%, 2.257%, 57.50% and 73.80%). In short, the results were exhibited in **Figure 4A and 4B**, proving that compound **5n** could induce A375 cell apoptosis.

2.6 Compound 5n induced cell cycle arrest in dose- and time-dependent manner

It was found that compound **5n** could induce cell cycle arrest and mitotic blocking of A375 cells by further experiments. A375 cells were treated with compound **5n** at various doses (0, 1, 3, or 10 μM) for 24 h, or with compound **5n** (3 μM) for various times (0, 12, 24, 36 h). The results, as shown in **Figure 5,** demonstrated that compound **5n** induced a gradual accumulation of A375 cells in G1 phase in a dose- and time-dependent manner. As a result, we could see that compound **5n** could induce cell arrest in the G1 period of the cell cycle and blocking cell mitosis.

2.7 Western blot revealed 5n could interfere the B-Raf^{V600E}-mediated pathways

While the abnormally activated ERK pathway caused by B-Raf^{V600E} results in the phosphorylated level of MEK and ERK increased, effective B-Raf^{V600E} inhibitors shall block the pathway and down-regulate the amount of pMEK and pERK. The effect of **5n** on MEK and ERK phosphorylation was investigated in A375 cell line expressing B-Raf^{V600E} and WM1361 cell line expressing B-Raf^{WT}. Cells were treated with different concentrations (0 μM, 0.03 μM, 0.1 μM and 0.3 μM) of **5n**, and the inhibitory activity was compared with that of vemurafenib. As shown in **Figure 6**, **5n** markedly suppressed the phosphorylation of MEK and ERK in a dose-dependent manner in A375 cells, with similar inhibitory effects can be found in vemurafenib group (**Figure 7**). Subsequently, the inhibition of **5n** to MEK and ERK phosphorylation were also evaluated against WM1361 cells expressing B-Raf^{WT}. While the paradoxical effect of vemurafenib at different concentrations was reported, no such responses of **5n** were observed in the B-Raf^{WT}-bearing WM1361 cells at concentrations up to 0.3 μM, as shown in **Figure 8**. Also as a control, no differences were noted for total ERK1/2 or MEK1/2 protein levels in this experiment.

2.8 Mitochondrial membrane potential analysis

According to the experiment, with the increase of concentration of compound **5n**, red fluorescence gradually weakened, and green fluorescence gradually strengthened. The results indicated that after treating A375 cells with gradient concentrations (0, 1, 3 or 10 μM) of compound **5n** for 12 h, the percentage of red fluorescence cells was markedly decreased in a

dose-dependent manner (with percentage of 92.84%, 89.60%, 75.80% and 25.10%). Meanwhile the percentage of red fluorescence cells was markedly increased in a dose-dependent manner (with percentage of 7.16%, 10.40%, 24.20% and 74.90%) as shown in **Figure 9**. Indicating that the mitochondrial membrane potential from high to low, there is a downward trend. Decrease of mitochondrial membrane potential is an important phenomenon in the early stage of apoptosis. It can be seen that compound **5n** can lead to changes in mitochondrial membrane potential of A375 cells, causing early apoptosis of cells.

3 Conclusion

In this study, we established a fragment library by extracting the known endogenous ligands from the protein-ligand complexes. On the basis of the protein structure analysis, we used the MCSS simulation to bind the copies of molecular fragment to the B-Raf activity pocket, and the copies with best conformation and optimal orientation were selected. Finally, the acquired lead-like compounds were screened for novelty primarily, and then docked iteratively to estimate the binding potency with the enzyme. Above all, the results obtained from this study suggest that our target skeleton may serve as a novel scaffold for the further development of more potent and selective B-RAF^{V600E} inhibitors that use as mutant B-RAF dependent melanoma therapeutic agents. In short, the study shows that our design method and design intent are valid, and we can use the MCSS simulation to carry out the FBDD strategy to design a new inhibitor in other drug design campaigns. It is hoped that this study may provide reference for the design of novel small molecule inhibitors by using MCSS simulation to achieve FBDD strategy.

Disclosure of potential conflicts of interest

The authors disclose that there is no potential conflict of interest.

Acknowledgement

This work was supported by National Science & Technology Supporting Project (No. 2015BAD16B07) and supported by the National Undergraduate Innovation Program and the National Natural Science Foundation of China (No. J1210026), and supported by the Research Innovation Program for College Graduates of Jiangsu Province in 2016 (No. SJZZ16_0014).

Reference

1. Kim E K, Choi E J. Pathological roles of MAPK signaling pathways in human diseases[J]. *Biochimica et Biophysica Acta (BBA)-Molecular Basis of Disease*, 2010, 1802(4): 396-405.

2. Sekine Y, Takeda K, Ichijo H. The ASK1-MAP kinase signaling in ER stress and neurodegenerative diseases[J]. *Current Molecular Medicine*, 2006, 6(1): 87-97.

3. Henry, J. R., Kaufman, M. D., Peng, S.-B., Ahn, Y. M., Caldwell, T. M., Vogeti, L., Telikepalli, H., Lu, W.-P., Hood, M. M., and Rutkoski, T. J. (2015) Discovery of 1-(3, 3-Dimethylbutyl)-3-(2-fluoro-4-methyl-5-(7-methyl-2-(methylamino) pyrido [2, 3-d] pyrimidin-6-yl) phenyl) urea (LY3009120) as a Pan-RAF Inhibitor with Minimal Paradoxical Activation and Activity against B-RAF or RAS Mutant Tumor Cells[J], *Journal of Medicinal Chemistry*, 58, 4165-4179.

4. Xia Q, Hu Q, Wang H, et al. Induction of COX-2-PGE2 synthesis by activation of the MAPK/ERK pathway contributes to neuronal death triggered by TDP-43-depleted microglia[J]. *Cell Death & Disease*, 2015, 6(3): e1702.

5. McCubrey J A, Steelman L S, Abrams S L, et al. Roles of the RAF/MEK/ERK and PI3K/PTEN/AKT pathways in malignant transformation and drug resistance[J]. *Advances in Enzyme Regulation*, 2006, 46(1): 249-279.

6. Chappell W H, Steelman L S, Long J M, et al. Ras/Raf/MEK/ERK and PI3K/PTEN/Akt/mTOR inhibitors: rationale and importance to inhibiting these pathways in human health[J]. *Oncotarget*, 2011, 2(3): 135-164.

7. Nucera C, Goldfarb M, Hodin R, et al. Role of B-Raf V600E in differentiated thyroid cancer and preclinical validation of compounds against B-Raf V600E[J]. *Biochimica et Biophysica Acta (BBA)-Reviews on Cancer*, 2009, 1795(2): 152-161.

8. Long G V, Wilmott J S, Capper D, et al. Immunohistochemistry is highly sensitive and specific for the detection of V600E B-RAF mutation in melanoma[J]. *The American Journal of Surgical Pathology*, 2013, 37(1): 61-65.

9. Kimura E T, Nikiforova M N, Zhu Z, et al. High prevalence of B-RAF mutations in thyroid cancer[J]. *Cancer Research*, 2003, 63(7): 1454-1457.

10. Roskoski R. Classification of small molecule protein kinase inhibitors based upon the structures of their drug-enzyme complexes[J]. *Pharmacological Research*, 2016, 103: 26-48.

11. Roskoski R. ErbB/HER protein-tyrosine kinases: Structures and small molecule inhibitors[J]. *Pharmacological Research*, 2014, 87: 42-59.

12. Wu P, Nielsen T E, Clausen M H. FDA-approved small-molecule kinase inhibitors[J]. *Trends in Pharmacological Sciences*, 2015, 36(7): 422-439.

13. Choi, J., Landrette, S. F., Wang, T., Evans, P., Bacchiocchi, A., Bjornson, R., Cheng, E., Stiegler, A. L., Gathiaka, S., and Acevedo, O. (2014) Identification of PLX4032-resistance mechanisms and implications for novel RAF inhibitors[J], *Pigment Cell & Melanoma Research*, 27, 253-262.

14. Horbert, R., Pinchuk, B., Davies, P., Alessi, D., and Peifer, C. (2015) Photoactivatable Prodrugs of Antimelanoma Agent Vemurafenib[J], *ACS Chemical Biology* 10, 2099-2107.

15. Wasko M J, Pellegrene K A, Madura J D, et al. A role for fragment-based drug design in developing novel lead compounds for central nervous system targets[J]. *Frontiers in Neurology*, 2015, 6.

16. Hall D R, Enyedy I J. Computational solvent mapping in structure-based drug design[J]. *Future Medicinal Chemistry*, 2015, 7(3): 337-353.

17. Rai S, Raj U, Tichkule S, et al. Recent Trends in In-silico Drug Discovery[J]. *International Journal for Computational Biology*, 2016, 5(1): 54-76.

18. Hung C L, Chen C C. Computational approaches for drug discovery[J]. *Drug Development Research*, 2014, 75(6): 412-418.

19. Steinbrecher T B, Dahlgren M, Cappel D, et al. Accurate binding free energy predictions in fragment optimization[J]. *Journal of Chemical Information and Modeling*, 2015, 55(11): 2411-2420.

20. Amaravadhi H, Baek K, Sup Yoon H. Revisiting de novo drug design: receptor based pharmacophore screening[J]. *Current Topics in Medicinal Chemistry*, 2014, 14(16): 1890-1898.

21. Zhao H, Caflisch A. Molecular dynamics in drug design[J]. *European Journal of Medicinal Chemistry*, 2015, 91: 4-14.

22. P. F. Wang, H. Y. Qiu, Z. F. Wang, Y. J. Zhang, Z. C. Wang, D. D. Li, H. L. Zhu. Identification of novel B-Raf^{V600E} inhibitors employing FBDD strategy[J]. *Biochem Pharmacol*, 2017, 132: 63-76.

Figure Captions

Figure 1. The hydrogen bonds between compound **5n** and key amino acid residues.

Figure 2. (A) The 3D binding mode of compound **5n** with B-Raf^{V600E} (PDB code: **4E26**). Compound **5n** is shown in purple; (B) Incorporating an overlay of vemurafinib and compound **5n** with B-Raf^{V600E}. Compound **5n** is shown in gray and vemurafinib is shown in cyan.

Figure 3. System and ligand root mean square deviation (RMSD) gained from MD simulations.

Table 1. The contribution of different binding energy and the total binding energy calculated by MM/PBSA.

Figure 4. (A) A375 cells treated with 0, 1, 3 and 10 μM **5n** for 24 h were collected and analyzed. The percentage of early apoptotic cells was shown in the lower right quadrant (Annexin V-FITC positive/PI negative cells), and late apoptotic cells are located in the upper right quadrant (Annexin V-FITC positive/PI positive cells); (B) A375 cells treated with 3 μM **5n** for 0, 12, 24, 36 h were collected and analyzed. The percentage of early apoptotic cells was shown in the lower right quadrant

(Annexin V-FITC positive/PI negative cells), and late apoptotic cells are located in the upper right quadrant (Annexin V-FITC positive/PI positive cells).

Figure 5. Effect of compound **5n** on cell-cycle progression of A375 cells was determined by flow cytometry analysis. (A) A375 cells treated with **5n** (0, 1, 3 and 10 μM) for 24 h; (B) A375 cells treated with **5n** (3 μM) for various times (0, 12, 24, 36 h). (G1 phase, green; S phase, yellow and G2/M phase, blue).

Figure 6. 5n blocked the ERK pathway in A375 cells. (A) 5n inhibited the phosphorylation of ERK in A375 melanoma cells bearing B-Raf^{V600E}; (B) 5n inhibited the phosphorylation of MEK in A375 melanoma cells bearing B-Raf^{V600E}.

Figure 7. Vemurafenib blocked the ERK pathway in A375 cells. (A) The effect of vemurafenib on the phosphorylation of ERK in A375 melanoma cells bearing B-Raf^{V600E}; (B) The effect of vemurafenib on the phosphorylation of MEK in A375 melanoma cells bearing B-Raf^{V600E}.

Figure 8. 5n slightly blocked the ERK pathway in WM1361 cells. (A) 5n slightly inhibited the phosphorylation of MEK in WM1361 melanoma cells bearing B-Raf^{WT}. (B) 5n slightly inhibited the phosphorylation of ERK in WM1361 melanoma cells bearing B-Raf^{WT}.

Figure 9. A375 cells treated with 0, 1, 3 and 10 μM **5n** for 12 h were collected and analyzed. (red fluorescence, high mitochondrial membrane potential; green fluorescence, low mitochondrial membrane potential).

Supporting Information

Experimental details for the compounds and biological assays.

Table S1. Structures of compounds 5a – 5p.

Table S2. The molecular properties of target compounds, vemurafenib.

Table S3. Compounds 5a – 5p potently inhibited proliferation of four cancer cells and B-Raf^{V600E} kinase activity.

Table S4. B-Raf^{WT} and C-Raf kinase selectivity of compound 5n and vemurafenib.

Figure S1. The revised structure of endogenous ligands extracted from B-Raf co-crystals.

Figure S2. The graph about CDOCKER INTERACTION ENERGY (-kcal/mol) of all compounds for B-Raf^{V600E}.

Table 1. The contribution of different binding energy and the total binding energy calculated by MM/PBSA.

Contributing Energy	Average Value (kJ/mol)
Van der Waal	-250.43 $\pm$ 4.33
Electrostatic	-41.00 $\pm$ 6.95
Polar Solvation	90.01 $\pm$ 5.25
Non-polar Solvation	-17.98 $\pm$ 0.89
Total Binding Energy	-219.40 $\pm$ 10.41

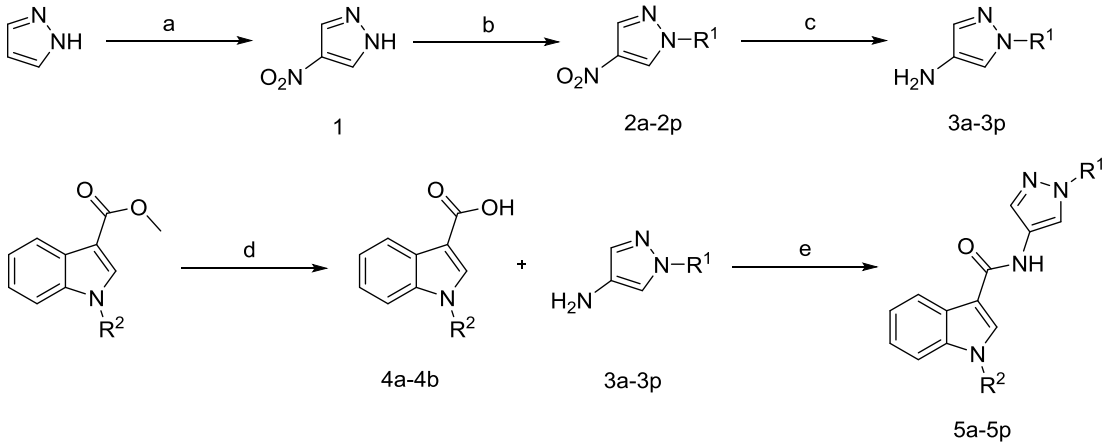

Scheme 1. The synthetic route for compounds **5a** – **5p.** (a) H_2SO_4, HNO_3, 60 °C, 2 h; (b) K_2CO_3, DMF, 25 °C, 16 h; or 1.0 equiv, Iodobenzenes, 0.1 equiv, 8-Hydroxyquinoline, 0.1 equiv, CuI, 2.0 equiv, K_2CO_3, DMSO , 135 °C, 20 h; or Sodium methoxide, DMF, 25 °C, overnight; (c) 80% Hydrazine hydrate, 10% Palladium charcoal, Ethanol, 80 °C, 10 min; (d) Potassium hydroxide, 65 °C, 2 h; (e) 1.0 equiv, EDC, 1.0 equiv, HOBt, 1.0 equiv, DMAP, Et_3N, DMF, rt.